

The Dependence of Prestellar Core Mass Distributions on the Structure of the Parental Cloud

Antonio Parravano^{1,2}, Néstor Sánchez³, Emilio J. Alfaro⁴

ABSTRACT

The mass distribution of prestellar cores is obtained for clouds with arbitrary internal mass distributions using a selection criterion based on the thermal and turbulent Jeans mass and applied hierarchically from small to large scales. We have checked this methodology comparing our results for a lognormal density PDF with the theoretical CMF derived by Hennebelle & Chabrier, namely a power-law at large scales and a log-normal cutoff at low scales, but our method can be applied to any mass distributions representing a star-forming cloud. This methodology enables us to connect the parental cloud structure with the mass distribution of the cores and their spatial distribution, providing an efficient tool for investigating the physical properties of the molecular clouds that give rise to the prestellar core distributions observed. Simulated fBm clouds with the Hurst exponent close to the value $H = 1/3$ give the best agreement with the theoretical CMF derived by Hennebelle & Chabrier and Chabrier's system IMF. Likewise, the spatial distribution of the cores derived from our methodology show a surface density of companions compatible with those observed in Trapezium and Ophiucus star-forming regions. This method also allows us to analyze the properties of the mass distribution of cores for different realizations. We found that the variations in the number of cores formed in different realizations of fBm clouds (with the same Hurst exponent) are much larger than the expected root \mathcal{N} statistical fluctuations, increasing with H .

Subject headings: Stars: formation — Stars: luminosity function, mass function — ISM: evolution — ISM: structure

¹Universidad de Los Andes, Centro De Física Fundamental, Mérida, Venezuela

²Instituto de Estudios Sociales Avanzados (IESA-CSIC), Córdoba, Spain

³S.D. Astronomía y Geodesia, Fac. CC. Matemáticas, Universidad Complutense de Madrid, Spain

⁴Instituto de Astrofísica de Andalucía (CSIC), Granada, Spain

1. Introduction

Is the stellar Initial Mass Function (IMF) universal? This question has been in the literature for a long time, and is now extended to the core mass function (CMF) since a close relation between the IMF and the CMF has been recognized (Motte et al. 1998; Testi & Sargent 1998; Alves et al. 2007; Chabrier & Hennebelle 2010; Michel et al. 2011). Compared to the CMF, the mass function of stellar systems seems to be shifted to lower masses by a factor that does not depend on the core mass. The currently favored conversion efficiency value of the progenitor core mass to the stellar system is $\sim 1/3$. However, the origin of this conversion efficiency is still controversial (Adams & Fatuzzo 1996; Matzner & McKee 2000; Enoch et al. 2008; Dib et al. 2011). Significant variations in the mass function of young clusters are observed in the disk of the Galaxy (e.g., Scalo 1998), but most of these variations are consistent with random sampling from a universal IMF (Elmegreen 1997, 1999; Kroupa 2002; Bastian et al. 2010; Parravano et al. 2011). The non-linear processes involved in the star formation process determine on the one hand the universal form of the IMF and on the other hand the range of expected variations of the mass function around this universal form. These fluctuations arise naturally in IMF models based on deterministic chaos (Sanchez & Parravano 1999) and are also observed in three-dimensional hydrodynamic simulations. Recently Girichidis et al. (2011) performed a parameter study of the fragmentation properties of collapsing isothermal gas cores with different initial conditions and showed that the density profile strongly determines the number of formed stars, the onset of star formation, the stellar mass distribution, and the spatial stellar distribution. Furthermore, the random setup of the turbulent velocity field in SPH simulation has a major impact in the different morphology of the filamentary structure, and consequently on the number of sink particles (as shown by Girichidis et al. 2011, 2012a,b).

The ever increasing resolution of magnetohydrodynamic numerical simulations will provide the answer to many of these questions (Elmegreen 2011). Nevertheless, theoretical IMF models, such as those proposed by Padoan et al. (1997); Padoan & Nordlund (2002) or Hennebelle & Chabrier (2008, 2009), provide analytical solutions that help elucidate the contribution of the various physical processes involved, but, to obtain these analytic solutions it is necessary to adopt a series of assumptions that limit their application to specific cases. The predictions of these theories have been compared to the numerical data from simulations. In particular, Padoan & Nordlund (2004) and Padoan et al. (2007) compared the analytical solutions of their theory to numerical simulations. Schmidt et al. (2010) have also compared the results from their simulations to the predictions of these theories and have shown how the clump mass distribution depends on the turbulence driving mechanism. In between these two approaches are the phenomenological models, such as the one presented here, that allow one to address some of the questions stated above, in particular, that of

sensitivity to the initial conditions. The method consists of a selection criterion based on the thermal and turbulent Jeans mass which is applied hierarchically from small to large scales.

1.1. Aim of the Paper

The methodology proposed in this work enables a direct connection between the structure of molecular clouds and the distributions of generated cores in both mass and space. Thus our first aim is to check that the results obtained using our methodology are consistent with those obtained using other methods proposed in the literature and that have produced reliable results. In particular, we will compare our results for a lognormal density PDF with the theoretical CMF derived by Hennebelle & Chabrier (2008), but using two different spatial distributions of the cloud mass: a) a random cloud, and b) what we have called a “corner” distribution where the voxel mass decreases with the distance to a preselected corner. This exercise allows us to evaluate the virtue of the method and how the geometry of the cloud defines the dependence of the standard deviation of the lognormal density PDF with the smoothing scale R . We have chosen these two very different spatial structures so as to make it clear how the analytic formulation of HC08 and the phenomenology presented here are connected through the scale dependence of the density PDF.

Second, we will explore the formation of cores for different parent clouds, but considering that the geometry that best describes the spatial structure of the clouds is fractal. Observations of close star-forming clouds indicate that the mass distribution in them can be described as having a fractal structure (Falgarone et al. 1992; Sanchez et al. 2005). The analysis will be carried out for fractional Brownian motion (fBm) clouds with a wide range of fractal dimensions. Specifically, we will focus on the comparative analysis of the following properties: a) Empirical dependence of density PDF on the smoothing scale; b) Mass distribution of the cores; c) Spatial distribution of the generated cores as measured by the surface density of companions, and, d) Cloud core properties averaged over several realizations for each H .

The paper is organized into five sections, this introduction being the first. §2 describes the method and defines the main physical variables of the problem and their range of values in our simulations. In §3 we check the virtue of our methodology in reproducing the CMF derived analytically by Hennebelle & Chabrier (2008), and in §4, we show the application of this methodology to fractal clouds generated as fBm clouds with different Hurst exponents and compare the results with previous approaches to the same physical systems. Finally, §5 is devoted to summarizing the main conclusions.

2. A Discrete Method for a Hierarchical Collapsing Sequence (HCS Method)

Following the nomenclature in McKee & Tan (2003) we define a star-forming clump as a massive region of molecular gas out of which a star cluster is forming; a core is a region of molecular gas that will form a single star (or a multiple-star system such as a binary). The resolution at which a distribution of matter is described can be limited by the procedure used to generate or measure the distribution, the capacity of storage of information, or simply can be chosen to meet a given level of description. In our case, the distribution of matter is given in a three-dimensional lattice cube of length L with N_{vox}^3 identical cubic voxels. The volume associated with each voxel is l_{vox}^3 , where $l_{vox} = L/N_{vox}$. The mass of gas contained in a voxel centered at coordinates $\vec{r} = l_{vox} \times [i\hat{x}, j\hat{y}, k\hat{z}]$ is denoted as $m_{i,j,k}$, where i, j and k run from 1 to N_{vox} .

If we assume that the densest voxel contains a mass m_{max} , and that the physical conditions in that voxel are such that it is gravitationally unstable¹, (i.e. the Jeans length equals l_{vox}), then the thermal Jeans mass $M_{J,th}$ ($\propto \rho^{-1/2}$) for a larger cube of d^3 voxels is

$$M_{J,th} = \frac{m_{max}^{3/2}}{\sqrt{m_{cube}/d^3}}, \quad (1)$$

where $m_{cube} = \sum_{i,j,k \in v} m_{i,j,k}$ is the mass contained in the volume v whose shape is a cube of side $d \times l_{vox}$. Note that we are implicitly assuming that the temperature and the molecular weight are the same in the d^3 voxels in the cube.

The turbulent Jeans mass can be expressed in terms of the thermal Jeans mass as

$$M_{J,turb} = M_{J,th} \frac{V_0^3}{3^{3/2} C_s^3} \left(\frac{R}{1\text{pc}} \right)^{3\eta} = M_{J,th} \left(\frac{d}{d_{eq}} \right)^{3\eta}, \quad (2)$$

where d_{eq} is the length (in l_{vox} units) at which the thermal support and the turbulent support are equal, $V_0 \simeq 1 \text{ km s}^{-1}$ is the turbulent rms velocity at 1 pc scale and $C_s = \sqrt{\frac{\gamma_g kT}{\mu m_H}} \simeq 0.22 (T/10\text{K})^{1/2} (\mu/2.33)^{-1/2} \text{ km/s}$ is the sound speed, where γ_g is the adiabatic index and μ is the molecular weight. The exponent η is the exponent of the Larson's (1981) velocity dispersion versus size relation and is related to the 3D power spectrum index of the velocity field $\eta = (n - 3)/2$ where $n = 11/3$ for the Kolmogorov case and 4 for the Burgers case. Kritsuk et al. (2007) estimate $n \sim 3.8 - 3.9$ ($\eta \sim 0.4 - 0.45$) from high resolution hydrodynamic simulations of isothermal supersonic turbulence, in agreement

¹Larson (1981) noted that “if there is a minimum size of bound condensations produced by supersonic compression processes, this may lead to a lower limit of the stellar masses”.

with Schmidt et al. (2009) who estimate $\eta \sim 0.45$ from simulations of supersonic isothermal turbulence driven by mostly compressive large-scale forcing. Federrath et al. (2010) showed that η depends on the nature of the turbulence forcing mechanism; 0.43 for solenoidal forcing and 0.47 for compressive forcing.

Myers & Fuller (1992) first included both thermal and nonthermal motions in a model of star formation in dense cores. McKee & Tan (2003) focused on the nonthermal part in their turbulent core model for massive star formation, but then showed how it is possible to smoothly join on to the thermal Jeans mass. Following Hennebelle & Chabrier (2008, hereafter HC08), who explicitly included both thermal and nonthermal motions, the Jeans mass can be expressed as

$$M_J = M_{J,th} \left\{ 1 + \left(\frac{d}{d_{eq}} \right)^{2\eta} \right\}^{3/2}. \quad (3)$$

To apply the Jeans criteria in eq. (3) to any cube in the array it is only necessary to know $m_{i,j,k}$ for all i, j, k in the array and the parameters m_{max} and d_{eq} . Note that the physical size l_{vox} of the voxels is not needed to determine whether a given cube is Jeans unstable. However, as shown below, the parameter d_{eq} depends on the physical conditions that determine l_{vox} and on the increase of the velocity dispersion with distance.

We propose here a procedure to obtain the prestellar core mass distribution which is based on a hierarchical collapsing sequence (hereafter the HCS method) in which the densest regions collapse first and form the smaller objects. At small scales, thermal support dominates and determines the core mass distribution at low masses, whereas, at the largest scales turbulence dominates the support and determines the mass distribution at high masses, as in the analytical theory of the IMF proposed by HC08. The discrete mass distribution $m_{i,j,k}$ is checked at all scales starting with the smallest, that is at the scale of one voxel, i.e. $d = 1$. By construction only the densest voxel (the one with mass m_{max}) is marginally unstable under the thermal Jeans criterion, however the small turbulent support is enough to suppress the collapse at one voxel scale. Then, cubes of side $d = 2$ are checked to find those that fulfill the condition $m_{cube} \geq M_J$. In the cubes fulfilling this condition, a core of mass $m_{core} = M_J$ is assumed to form giving rise to a stellar system of mass $m_* = \epsilon m_{core}$. The remaining gas $m_{cube} - \epsilon M_J$ is assumed to become inactive. After this, cubes of side $d = 3, 4, \dots, N_{vox}/2$ are considered consecutively. Note that the properties of the velocity field are not considered explicitly, but are taken into account implicitly by means of the parameters d_{eq} and η .

To fix the voxel length l_{vox} we use the assumption that the mass m_{max} contained in the densest voxel is gravitationally marginally stable. The radius of a Bonnor-Ebert sphere is

$R_{BE} \simeq 0.486 R_G$ and the thermal Jeans length is $l_{J,th} = \sqrt{\pi} R_G$, where R_G , the gravitational length (McKee & Ostriker 2007), is

$$R_G = \sigma_{th}/(G\rho)^{1/2} \simeq 0.21 \left(\frac{T}{10\text{K}} \right)^{1/2} \left(\frac{\mu}{2.33} \right)^{-1/2} \left(\frac{n_H}{10^4 \text{cm}^{-3}} \right)^{-1/2}, \quad (4)$$

and where n_H is the hydrogen nucleus number density.

Since the density in the densest voxel is $n_H \simeq 41 \left(\frac{m_{max}}{1M_\odot} \right) / \left(\frac{l_{vox}}{1\text{pc}} \right)^3 \text{cm}^{-3}$, the voxel length is

$$l_{vox} = l_1 \left(\frac{m_{max}}{1M_\odot} \right) \left(\frac{10\text{K}}{T} \frac{\mu}{2.33} \right) \text{pc}, \quad (5)$$

where $l_1 = 0.15$ if $l_{vox}^3 = \frac{4}{3}\pi R_{BE}^3$. Note that this value is close to the value $l_1 = 0.18$ obtained if $l_{vox}^3 = \frac{4}{3}\pi \left(\frac{l_{J,th}}{4} \right)^3$. We adopt $l_1 = 0.15$ here.²

Finally, the parameter d_{eq} depends on the turbulent rms velocity which is assumed to increase with the size R of the region following the Larson relation $\langle V_{rms}^2 \rangle = V_0^2 \times \left(\frac{R}{1\text{pc}} \right)^{2\eta}$, where $V_0 \simeq 1 \text{ km s}^{-1}$. The value R_{eq} at which thermal and turbulent support are equal can be expressed in terms of the sound speed C_s as $R_{eq}/1\text{pc} = (\sqrt{3}C_s/V_0)^{\frac{1}{\eta}}$. Therefore, in terms of the Mach number at 1 pc scale $\mathcal{M}_{1\text{pc}} = V_0/C_s$, the number of voxels d_{eq} for which thermal and turbulent support are equal is

$$d_{eq} \equiv R_{eq}/l_{vox} = \left(\sqrt{3}/\mathcal{M}_{1\text{pc}} \right)^{\frac{1}{\eta}} / (l_{vox}/1\text{pc}). \quad (6)$$

We apply the HCS procedure first to mass distributions with a log-normal density probability distribution function (PDF) in order to compare our numerical results to the analytical CMFs derived by HC08. Later the procedure is applied to fractal clouds with density PDFs that are not necessarily log-normal.

3. Comparison to the HC08 Analytical CMFs Theory

The analytical theory for the IMF developed in HC08 is based on an extension of the Press & Schechter (1974) statistical formalism applied in cosmology. When applied to the

² If we consider that the smallest single brown dwarf that can be formed has a mass of the order of $0.02 M_\odot$ and the progenitor core is about three times this mass, then $m_{max} \sim 0.06 M_\odot$. For this value of m_{max} and the fiducial values $T = 10 \text{ K}$ and $\mu = 2.33$, eq. (5) gives $l_{vox} = 0.009 \text{ pc}$, a value that roughly agrees with the value predicted by Larson's law for this mass (Larson 1981; Kauffmann et al. 2010).

mass function of molecular cloud cores, the original Press-Schechter formalism has the problem that structures inside structures are not counted. This cloud-in-cloud problem was overcome by assuming a conditional probability of finding a collapsed region of mass scale M inside a collapsed region of mass scale M' (Inutsuka 2001, and references therein). Additionally, in the Press-Schechter theory the structures are identified with over-densities in a random field of density fluctuations; i.e. a normal distribution in density. Instead, HC08 assume a log-normal distribution in density, as suggested by numerical simulations of non-self-gravitating supersonic isothermal turbulence (Vazquez-Semadeni 1994; Padoan et al. 1997; Passot & Vazquez-Semadeni 1998; Ostriker et al. 2001; Kritsuk et al. 2007) and observations (Kainulainen et al. 2009, 2011). Finally, HC08 assume that at any smoothing scale R the mass distribution in the cloud is such that the density PDF is always log-normal but with a standard deviation $\sigma(R)$ that decreases with R as

$$\sigma^2(R) = \sigma_0^2 \left(1 - \left(\frac{R}{L_i} \right)^{2\eta} \right), \quad (7)$$

where L_i is the injection scale and σ_0 is the width of the density distribution at maximum resolution $R \ll L_i$. The density PDF at resolution R is then

$$P_R(\delta, R) = \frac{1}{\sqrt{2\pi\sigma^2(R)}} \exp\left[-\frac{[\delta - \frac{\sigma^2(R)}{2}]^2}{2\sigma^2(R)}\right], \quad (8)$$

where $\delta = \ln(\rho/\bar{\rho})$ and $\bar{\rho}$ is the cloud mean density. For this scale-dependent density PDF their theory identifies gravitationally-bound prestellar cores with regions that have a density threshold given by the requirement that a fluctuation contains at least one local (thermal or turbulent) Jeans mass. As before, the turbulent rms velocity is assumed to correlate with size R following the Larson power-law $\langle V_{\text{rms}}^2 \rangle = V_0^2 \times \left(\frac{R}{1\text{pc}} \right)^{2\eta}$. The places where the average density at scale R is larger than the density threshold contain more than one Jeans mass and are expected to form prestellar cores of mass smaller than or equal to the mass contained in that region. This is because at smaller scales it may happen that the region is not uniform but composed of smaller, denser regions embedded into a more diffuse medium. If these denser regions contain one Jeans mass, the end product of the collapse is likely to be a cluster of objects whose mass is close to the mass of the smaller/denser regions and not to the mass in the volume at scale R . Taking into account the probability of finding these unstable sub-structures, HC08 express their core mass function as:

$$\psi_{\text{HC}}(\tilde{m}) \equiv \frac{1}{\mathcal{N}_{\text{tot}}} \frac{d\mathcal{N}}{d \ln \tilde{m}} \propto \frac{1}{(\tilde{m}\tilde{R}^3)^{1/2}} \left[\frac{1 + (1 - \eta)\mathcal{M}_*^2 \tilde{R}^{2\eta}}{1 + (2\eta + 1)\mathcal{M}_*^2 \tilde{R}^{2\eta}} \right] \exp \left\{ -\frac{[\ln(\tilde{m}/\tilde{R}^3)]^2}{2\sigma_0^2} - \frac{\sigma_0^2}{8} \right\}, \quad (9)$$

where

$$\tilde{m} \equiv \frac{m}{m_{\text{J}}^0} = \tilde{R}(1 + \mathcal{M}_*^2 \tilde{R}^{2\eta}), \quad (10)$$

m_{J}^0 is the Jeans mass at the average cloud density, \tilde{R} is the radius of the clump in units of the Jeans length at the average cloud density, \mathcal{M}_* is the characteristic Mach number at the Jeans scale, and η ($\sim 0.4 - 0.45$) is the exponent of the linewidth-size relation. The $\psi_{\text{HC}}(\tilde{m})$ mass distribution in eqs. (9 - 10) represents the stellar IMF, whereas $\psi_{\text{HC}}(m)$ represents the CMF.

At low masses ($\tilde{m} < 1$), the form of ψ_{HC} is log-normal. At moderately high masses ($m \gtrsim m_{\text{J}}^0$) the IMF approaches the power law

$$\psi_{\text{HC}} \propto \tilde{m}^{-(\eta+2)/(2\eta+1)} \equiv \tilde{m}^{-\Gamma_{\text{HC}}} \quad (\tilde{m} \gtrsim 1), \quad (11)$$

which gives $\Gamma_{\text{HC}} \simeq 1.3$ for the value $\eta \simeq 0.4$ they adopt, in agreement with the Salpeter (1955) value. At very high masses ($\tilde{m} \gg 1$) the IMF drops off more steeply with mass, becoming a log-normal type distribution again. Their results for a non-isothermal equation of state are considerably more complicated, but they are qualitatively consistent with the isothermal theory (Hennebelle & Chabrier 2009).

Note that only the scale-dependent log-normal PDF of the density and the properties of turbulence are considered in the HC08 theory. The detailed spatial distribution of matter is irrelevant, even when, implicitly, their results refer to the kind of gas distributions associated with turbulence. Instead, the HCS method proposed here explicitly takes into account the spatial distribution of the matter, and as shown below, the resulting core mass distribution is sensitive to this distribution.

For the moment we do not consider the radiative feedback (Hollenbach & Tielens 1999; Gorti & Hollenbach 2002; Krumholz et al. 2007, 2011; Bate 2009, 2012; Price et al. 2009), but it is expected that its efficiency also greatly depends on the spatial distribution of the matter.

3.1. Artificial mass distributions with log-normal density PDFs: “corner” and “Random” clouds.

To compare with HC08 we first consider two extreme mass distributions that are useful for showing the importance of the spatial structure of the cloud on the resulting mass function of collapsing cores. The first is a “random cloud” in which the masses $m(i, j, k)$ and the positions (i, j, k) are uncorrelated. The second is a “corner cloud” in which the locations of

the mass voxels $m(i, j, k)$ are ordered in such a way that the density decreases as the sum $i + j + k$ increases.

Since the lattice is regular and the voxel size l_{vox} is fixed by m_{max} , the mass distribution of the voxels (that is the number of voxels with a given mass) is proportional to the density PDF, and therefore the standard deviation σ_0 is the same for the PDF of the masses $m(i, j, k)$ and for the PDF of the gas density, and has the same meaning as in eq. (9). The PDFs of the masses $m(i, j, k)$ in both types of clouds follow the same log-normal function

$$dN/d\ln m = \frac{N_{vox}^3}{\sigma_0 \sqrt{2\pi}} \exp\left[-\frac{[\ln(m/\bar{m}) - \frac{\sigma_0^2}{2}]^2}{2\sigma_0^2}\right], \quad (12)$$

where \bar{m} is the mean mass per voxel and the peak of the distribution occurs at $\ln(m_0) = \ln(\bar{m}) - \sigma_0^2/2$. However, the dependence of the standard deviation $\sigma(R)$ on the smoothing scale R is, as shown in Fig. 1, very different. The smooth gradients in the mass distribution of the “corner cloud” produce a $\sigma(R)$ that is close to the HC08 dependence in eq. (7). In the “random cloud” case, $\sigma(R)$ rapidly drops to zero due to the unphysical discontinuous densities that make the average density in any volume containing a relatively small number of voxels very close to $\bar{\rho}$.

3.2. Comparison of HC08 and HCS CMFs for equivalent clouds.

To compare the core mass function corresponding to a particular mass distribution $m_{i,j,k}$ with ψ_{HC} we have to determine the set of HC08 parameters (σ_0 , m_J^0 , \mathcal{M}_*) from the HCS input parameters (N_{vox} , m_{max} , T , μ , η).

The voxel size $l_{vox}(m_{max}, T, \mu)$ is calculated from eq. (5), and the mean cloud density is $\bar{n}_H = \sum m_{i,j,k}/(m_H L^3)$ with $L = N_{vox} \times l_{vox}$.

Following HC08 (see also Hennebelle & Chabrier 2009) the Mach number at the Jeans scale at the cloud mean density \bar{n}_H is

$$\mathcal{M}_*^2 \simeq (T/10\text{K})^{\eta-1} (\bar{n}_H/10^4\text{cm}^{-3})^{-\eta} \quad (13)$$

and the Jeans mass at the cloud mean density \bar{n}_H is

$$m_J^0 = m_1 (T/10\text{K})^{3/2} (\mu/2.33)^{-3/2} (\bar{n}_H/10^4\text{cm}^{-3})^{-1/2} M_\odot, \quad (14)$$

where the value of m_1 depends on the definition of the Jeans mass. HC08 adopt $m_1 \simeq 1$, but if m_J^0 is assumed to be the mass in a sphere of diameter $l_{J,th} = \sqrt{\pi} R_G$ then $m_1 \simeq 6.6$. If instead m_J^0 is assumed to be the mass in a sphere of diameter $l_{J,th}/2$ then $m_1 \simeq 0.8$, close to

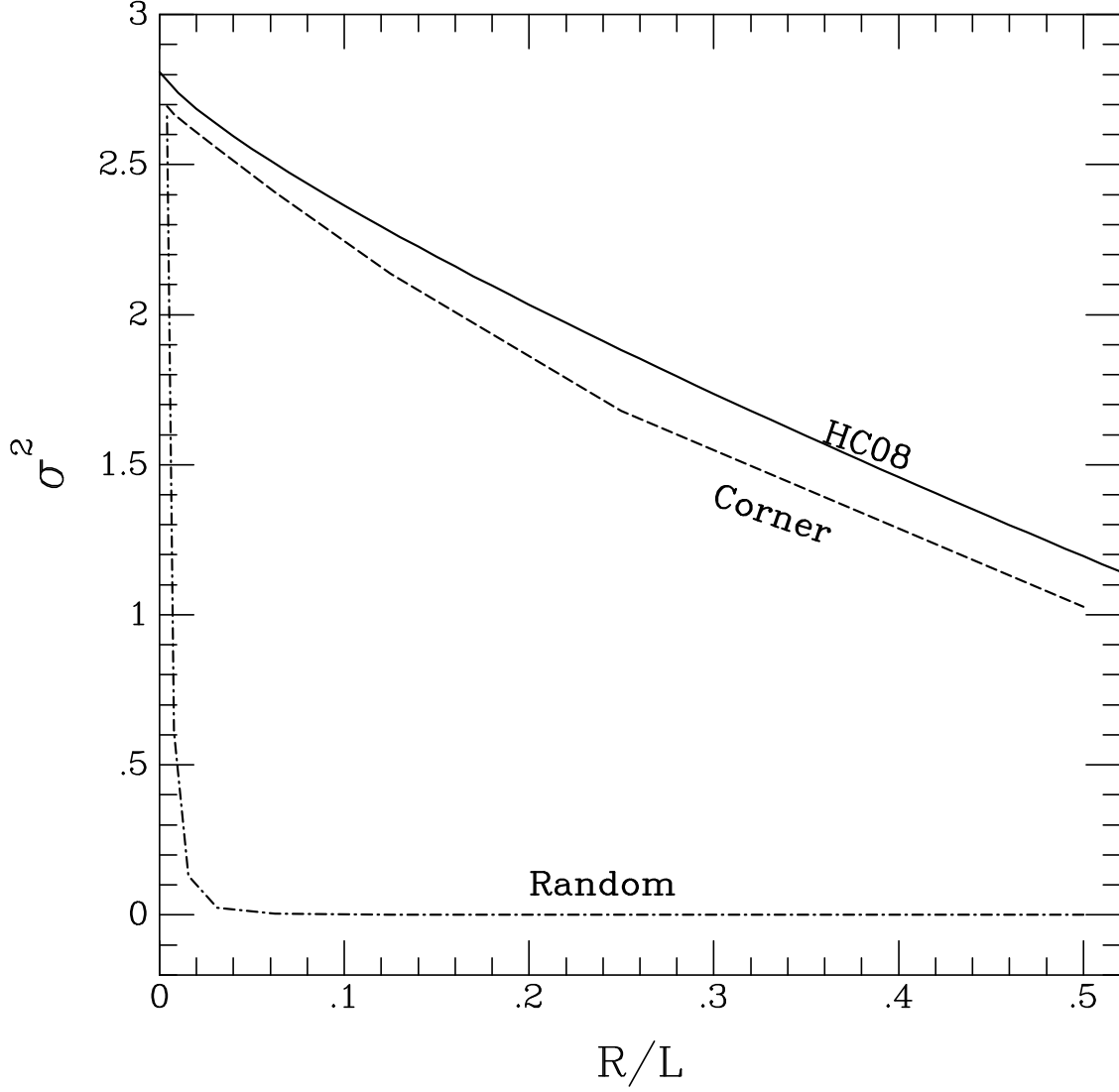


Fig. 1.— Dependence of the standard deviation on the smoothing scale for two different mass distributions and the dependence assumed by HC08 in eq. (7) with $L_i = L$ and σ_0 calculated from eqs. (15 - 16). The parameters in the three cases are $N_{vox} = 2^8$, $m_{max} = 0.07M_\odot$, $T = 10\text{K}$, $\mu = 2.33$ and $\eta = 0.4$, corresponding to the third case in Table 1.

the value adopted in HC08. We assume $m_1 = 1.08$, corresponding to the case in which m_j^0 is assumed to be the mass in a Bonnor-Ebert sphere.

The Mach number at the cloud scale $\mathcal{M} = \frac{V_0}{C_s}(\frac{L}{1\text{pc}})^\eta$ is

$$\mathcal{M} \simeq (1/0.22) (T/10\text{K})^{-1/2} (\mu/2.33)^{1/2} (L/1\text{pc})^\eta, \quad (15)$$

and the width of the density distribution σ_0 at the cloud scale is

$$\sigma_0^2 = \ln(1 + b^2 \mathcal{M}^2), \quad (16)$$

where $b^2 \approx 0.25$ (see also Hennebelle & Chabrier 2009).

For a given set of parameters σ_0 and m_{max} , the masses in the N_{vox}^3 voxels in the “random” or the “corner” clouds can be assigned following the log-normal distribution in eq. (12), requiring that the mass in the densest voxel is m_{max} . Then the resulting core mass function for $m_{i,j,k}$ can be compared to ψ_{HC} . However, what is the appropriate value for m_{max} to make the comparison? We assume that the appropriate value of m_{max} is the value for which the mean cloud density \bar{n}_H is such that the whole cloud is close to virial equilibrium; that is, the virial parameter (Larson 1981; Bertoldi & McKee 1992), defined as $\alpha_{\text{VIR}} = 5\sigma_{\text{vel}}^2 R / (GM_{cl}) \simeq 5(\frac{\Delta v}{2})^2 (L/2) / (GM_{cl})$ is equal to one. Therefore, $(M_{cl}/1M_\odot) \simeq 150(L/1\text{pc})^{2\eta+1}$ if $(\Delta v/1\text{km s}^{-1}) \simeq (L/1\text{pc})^\eta$. The cloud mass $M_{cl} = \sum m_{i,j,k}$ depends on the form of the density PDF, on the number of voxels in the lattice and on m_{max} . The lattice size L depends on m_{max} through $l_{vox}(m_{max})$ in eq. (5).

Table 1 gives the m_{max} values that fulfill the above two conditions when the PDF of the mass in voxels is log-normal. Table 1 also gives various derived quantities and the corresponding HC08 parameters. Note that the virial parameter is calculated omitting the effect of the pressure produced by the medium surrounding the cloud. Kainulainen et al. (2011) estimate that the pressures supporting the clumps against dispersal amount in total to about one third of the pressure driving their dispersal. Therefore, cloud masses in Table 1 exceed the Jeans masses in eq. 3 since $M_{J,th}$ is based on the stability of a Bonnor-Ebert sphere.

For the “corner cloud” and two array sizes, $N_{vox} = 128$ and 256, Figure 2 shows the histograms of the PDF of voxel masses $m_{i,j,k}$ and the core masses obtained with the HCS method. Figure 2 also shows the analytical PDF and core mass function from HC08; the dashed gray curve is ψ_{HC} from eq. (9) as function of $\tilde{m} = m/m_j^0$, whereas the continuous gray curve is not normalized to m_j^0 . Agreement with the non-normalized HC08 CMF is good for all cases in Table 1. The rapid falloff of the core mass function at low m is due to the fact that by construction we have set the most massive voxel to a mass of about 0.06, and that

TABLE 1
Properties of clouds with log-normal density PDFs

N_{vox}	T	m_{max}	d_{eq}	M_{cl}	L	\bar{n}_H	σ_0	\mathcal{M}	\mathcal{M}_*	m_J^0
	[K]	$[M_\odot]$		$[M_\odot]$	[pc]	$[\text{cm}^{-3}]$				$[M_\odot]$
64	10	0.109	5.67	156	1.05	5616	1.42	5.09	1.12	1.44
128	10	0.088	7.02	370	1.69	3166	1.53	6.17	1.26	1.92
256	10	0.070	8.83	862	2.69	1831	1.64	7.43	1.40	2.52
256	8	0.042	8.91	521	2.02	2622	1.64	7.40	1.40	1.51
256	12	0.106	8.79	1301	3.39	1375	1.64	7.44	1.41	3.83

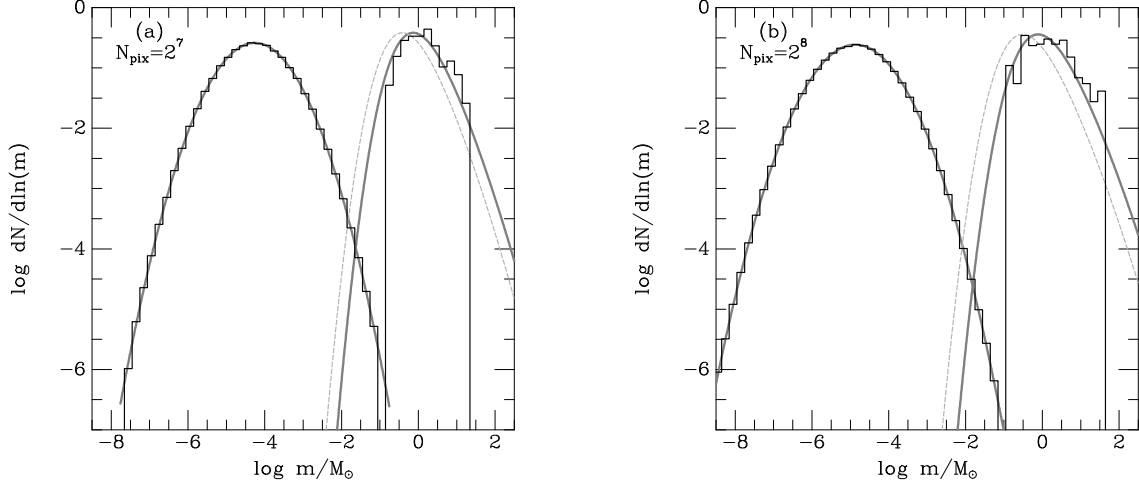


Fig. 2.— Histograms of the PDF of mass in voxels and the resulting core mass function for the “corner cloud” case for two array sizes, $N_{vox} = 128$ (a) and 256 (b). The parameter values are those in the second and third lines of Table 1. The continuous gray curve at the left of each panel is a log-normal with the appropriate values σ_0 and m_{max} . The continuous gray curve at the right of each panel is $\psi_{\text{HC}}(m)$ and the dashed gray curve is the normalized HC08 IMF $\psi_{\text{HC}}(m/m_J^0)$.

sets the minimum mass of a core. At high m the rapid falloff is because the highest mass of a core is limited by the mass of the cloud that remains after the formation of the smaller cores. Results very similar to those in Fig. 2 are obtained for spherically symmetric distributions in which the densest voxel with mass m_{max} is located at the center of the array and the mass of the remaining voxels decrease from the center in accord with the log-normal PDF. These results indicate that the HCS numerical method captures the main features of the HC08 analytical theory. However, the HCS method is not restricted to mass distributions with density PDFs following eqs. (7-8).

HC08 express their stellar IMF in terms of m_j^0 which is about $3 M_\odot$ for a mean cloud density $\bar{n}_H \sim 1000 \text{ cm}^{-3}$. Instead of normalizing masses to m_j^0 we assume that the non-normalized function $\psi_{\text{HC}}(m)$ represents CMF and that the mass function of stellar systems is shifted to lower masses by a factor ϵ of about $1/3$. The evolution of the CMF to the IMF has not been definitively established but magnetically-driven outflows (Matzner & McKee 2000) are expected to produce a mass independent efficiency factor in the range $30 - 50\%$; we assume a value of $\epsilon \simeq 1/3$. Note that our procedure for obtaining the stellar mass function for a particular gas distribution, as well as the theories of the IMF such as those of Padoan & Nordlund (2002) (see also Padoan et al. 2007) and HC08, predict the system IMF, whereas observations that cannot resolve close binaries determine an effective IMF since unresolved binaries are counted as single stars with an effective mass. The determination of the individual star IMF, in which each star that is a member of a multiple system is counted separately (Parravano et al. 2011), is beyond the scope of the present study. The fraction of the cloud mass that eventually becomes collapsing cores (~ 0.6), as well as the number of these cores, depends weakly on the gas temperature but the mean core mass is proportional to $(T/10\text{K})^{1+1/\eta}$.

Contrary to the “corner cloud” or the spherically symmetric distributions, a “random cloud” that has the same density PDF does not produce low mass collapsing cores, showing that the spatial structure of the cloud is very important not only for the spatial distribution of the protostellar objects, but also for the efficiency and mass function of the star forming objects. For the PDF of mass in voxels in Fig. (2-b), the lowest mass core that collapses in the random cloud is $1.3 M_\odot \sim 20 m_{max}$, whereas for the corner cloud it is $0.12 M_\odot \sim 2 m_{max}$. If the virial parameter of the cloud is increased to $\alpha_{VIR} = 2.5$ (i.e. $M_{cl} \simeq 1000 M_\odot$ and $L \simeq 5$ pc), then the random cloud produces only a couple of high mass cores ($m \sim 100 M_\odot$) but the corner cloud still produces a similar number of cores as in the $\alpha_{VIR} = 1$ case.

It is important to point out that these results show that the dependence of the dispersion of the density PDF on the smoothing scale strongly affects the resulting mass distribution of collapsing cores. Federrath et al. (2010) showed that the density PDF in their simulations

are roughly consistent with log-normal distributions for both solenoidal and compressive forcings, even when the distributions clearly exhibit non-Gaussian higher-order moments. However, the dispersion of the density PDF is highly sensitive to the turbulence forcing, and therefore they conclude that the theoretical CMF/IMF derived in HC09 is strongly affected by the assumed turbulence forcing mechanism. In the following we consider fractal mass distributions with roughly log-normal distributions, but with adjustable $\sigma(R)$ functions.

4. Fractal Clouds

Fractal clouds are known to be a good representation of star forming regions (Sanchez et al. 2007a,b; Elmegreen 2002, 2010). These kinds of clouds are easy to construct by means of recurrence procedures that produce hierarchical self-similar mass distributions. Fractal distributions are observed over a wide range of scales, from dense cores to giant molecular clouds (Bergin & Tafalla 2007). In particular, numerical simulations of supersonic isothermal turbulence (Kritsuk et al. 2007; Federrath et al. 2009) showed that the density field has an approximately fractal structure.

We focus on fractional Brownian motion clouds (hereafter fBm clouds; Stutzki et al. 1998; Elmegreen 2002; Miville-Deschenes et al. 2003; Sanchez et al. 2010) that have been used to represent the internal structure of molecular clouds. The fBm clouds are generated following the procedure described in Miville-Deschenes et al. (2003). That is, a field with Gaussian distribution intensity $\tilde{I}_{i,j,k}$ is obtained by first filling a lattice in wavenumber space (k_x, k_y, k_z) with a random phase and Fourier amplitudes proportional to $|\vec{k}|^{-(H+E/2)}$, where $|\vec{k}| = (k_x^2 + k_y^2 + k_z^2)^{1/2}$, H is the drift (or Hurst) exponent, and E is the dimension of the lattice. Subsequently, an inverse fast Fourier transform is applied to generate an intensity distribution $I_{i,j,k}$ in real space with a Gaussian intensity distribution. Since intensities must be real values, the Fourier amplitudes and phases in the wave number space have to match the appropriate symmetry conditions (Stutzki et al. 1998). The exponent H corresponds to a power spectrum of the intensity distribution $\gamma = 2H + E$. High resolution numerical experiments of supersonic isothermal turbulence driven by solenoidal forcing, obtained by Federrath et al. (2009), have been characterized by a Hurst exponent $H = 0.39$, corresponding to a box counting dimension $D_b \simeq 2.61$. Even when the three dimensional density and velocity fields are correlated (Miville-Deschenes et al. 2003), their relation strongly depends on the physical processes involved in the gas dynamics, for example on the energy injection mechanism as shown in Federrath et al. (2009). HC09 theory takes the exponent of the power spectrum of the density and velocity fields into account, but in their CMF analytical solutions the two exponents are assumed to be equal. This assumption is used in the previous

section to compare our method with HC09 (i.e. through the exponent η in eq. (7)). Note that if the two exponents are assumed to be equal, $H = 1/3$ for a dissipationless cascade of energy through an incompressible fluid (i.e. $\gamma = 11/3$ for $E = 3$). In this section, for the application of our method to fBm clouds, we use the quantities η and H to parameterize separately the velocity and the density fields; the first parameterize the turbulent support, and the second determine average properties of the mass distribution in fBm clouds, including $\sigma(R)$. FBm clouds have a two-point correlation function of the intensity $G_I(\lambda) \propto \lambda^{2H}$ (Stutzki et al. 1998), so that the mean variation over distance λ is $\Delta_I(\lambda) \propto \lambda^H$.

To generate a three-dimensional turbulent fractal cloud with a log-normal density distribution we follow Elmegreen (2002); that is, the Gaussian intensity distribution $I_{i,j,k}$ is exponentiated to generate a density distribution with a log-normal PDF. The masses $m_{i,j,k}$ in the lattice are $m_{i,j,k} = m_{max} \exp[\alpha (\frac{I_{i,j,k}}{I_{max}} - 1)]$, where I_{max} is the maximum value of intensities $I_{i,j,k}$ and α is the contrast factor. Since for a given α the intensity $I_{i,j,k}$ is proportional to $\ln(m_{i,j,k})$, the mean variation of $\ln(m)$ over distance λ is proportional to λ^H . That is, small values of H produce very rough structures, whereas very smooth structures are produced with H close to 1. Elmegreen (2002) restrict their results to the case $H = 1/3$.

By construction the densest voxel has a mass m_{max} . The total mass in the lattice M_{cl} , and therefore the mean mass per voxel \bar{m} , depends on α and H . However, due to the finite size of the lattice, two realizations using the same parameter values α and H but different randomization of the phases in general do not contain the same total mass M_{cl} . Also, due to the finite size of the array, the density PDF departs from the log-normal form, especially at low densities and large values of H . To compare the results among fBm clouds we adjust the value of α in each realization in order to have the same mass M_{cl} and the same maximum voxel mass m_{max} in the lattice.

Figure (3) shows $\sigma^2(R/L)$ for fBm clouds with various values of the Hurst exponent H . Each curve represents the average over 10 realizations and the error bars indicate the 10 and 90 percentiles. As in Fig. 1 the cloud mass M_{cl} and the value of σ_0 in the HC08 theory (eq.7) are the values corresponding to the case in the third line of Table 1. The dashed area represents the values of σ^2 given by eq.(7) with an injection scale length in the range $L/2 \leq L_i \leq 2L$.

Figure (4) shows the mass distribution of the cores formed in 20 different simulations with the same parameters H and m_{max} , and the contrast factor α adjusted to always produce the same cloud mass. The agreement with $\psi_{HC}(m)$ is much better for the case $H = 1/3$ than for $H = 1/6$. When $H = 1/6$ there is a clear excess of high mass cores compared to $\psi_{HC}(m)$, which can be understood in terms of the dependence σ^2 on R . As shown in Fig. 3, except for $R/L \lesssim 0.03$ the curve $\sigma^2(R; H = 1/6)$ is below the HC08 curve $\sigma_0^2(1 - (R/L)^{2\eta})$. When $\sigma^2(R)$

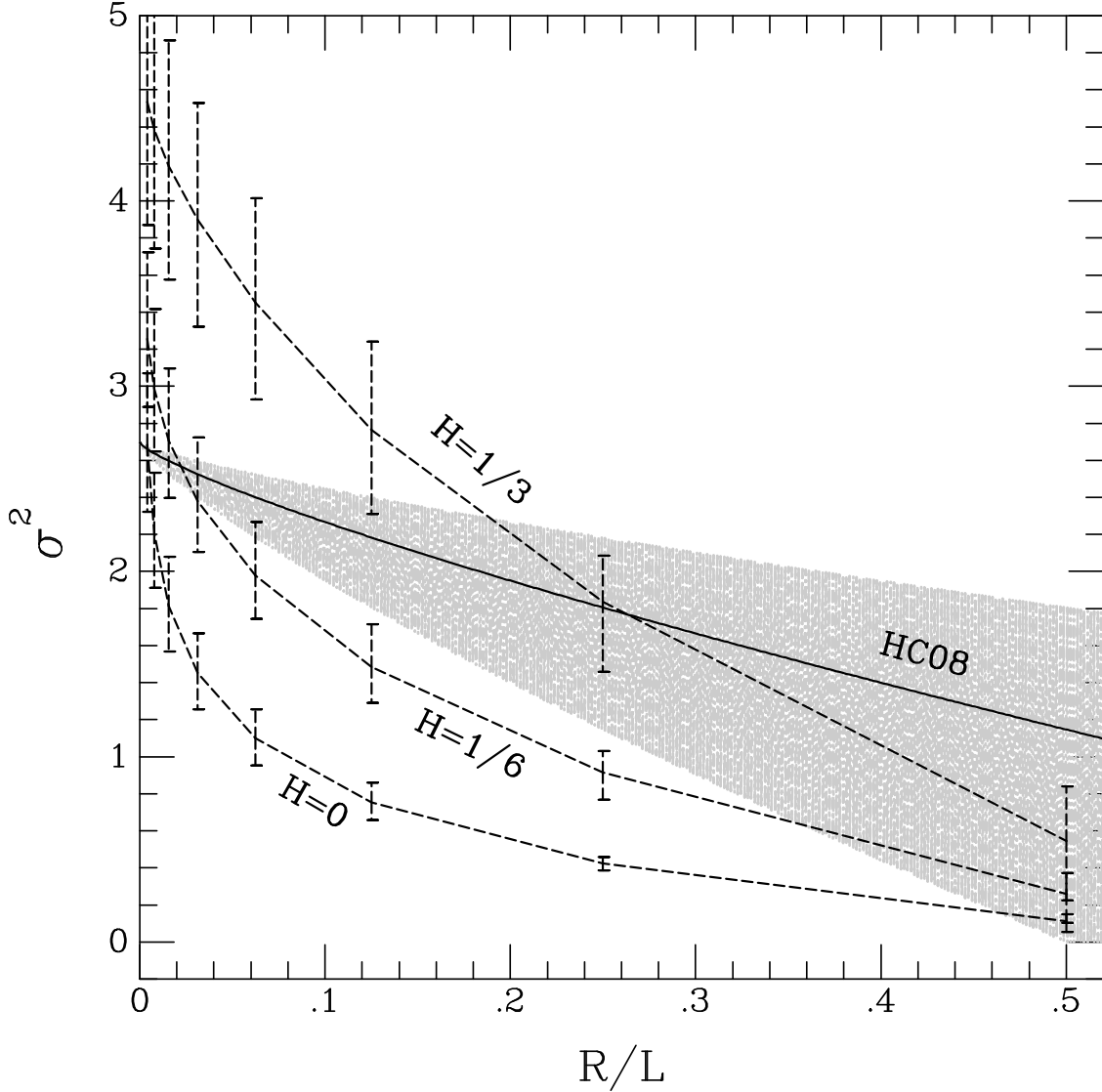


Fig. 3.— Dependence of the standard deviation on the smoothing scale $\sigma^2(R)$ in fBm clouds with three different values of the Hurst parameter H . Each curve with error bars corresponds to the average value for ten fBm clouds with the same H . The dashed area represents the HC08 values of σ^2 given by eq. (7) with an injection scale length in the range $L/2 \leq L_i \leq 2L$. The curve with the label HC08 corresponds to eq. (7) with $L_i = L$ and σ_0 calculated from eqs. (15 - 16). The parameters used are $N_{vox} = 2^8$, $m_{max} = 0.07 M_\odot$, $T = 10\text{K}$, $\mu = 2.33$ and $\eta = 0.4$, which correspond to $L = 2.7 \text{ pc}$, $M_{cl} = 860 M_\odot$, $\sigma_0 = 1.64$, as in the case of the third line of Table 1.

is small, the density PDF is a narrow distribution around $\bar{\rho}$ and at these densities and sizes only massive cores can form. Note that the curve $\sigma^2(R; H = 1/3)$ intersects the HC08 curve at a larger scale and that is why a fBm cloud with $H = 1/3$ produces in general more low-mass cores than that predicted by the HC08 theory. These results highlight the importance of the spatial distribution of the gas on the resulting mass distribution of collapsing objects.

A complex interplay of physical processes determines the final mass of the stars that form from a particular configuration of cores in a star-forming region. However, the scaling observed between the CMF and the stellar IMF indicate that some average relations between these two distributions can be established. For example, the fraction $F_{h,ms}$ of individual main-sequence stars that will end as core collapse supernovae or the mean mass \bar{m}_* of stars in the IMF can be estimated in terms of core to stellar system efficiency ($\epsilon \sim 1/3$, Matzner & McKee 2000), and the dependence of the binary fraction on the system mass (Lada 2006).

The stellar mean mass can be approximated as $\bar{m}_* \approx (\epsilon/R_s)\bar{m}_{core}$, where R_s is the mean number of stars per system in the IMF. In other words, R_s is defined as the ratio of the total number of stars to the total number of systems (single star systems + multiple star systems). Parravano et al. (2011) estimate that the mean mass of the objects in the individual star IMF is $\bar{m}_* \simeq 0.75M_\odot$, so that, assuming that $R_s \simeq 1.3$ (Lada 2006), the corresponding mean core mass is $\bar{m}_{core} \approx 3M_\odot$. Note that this estimate of \bar{m}_{core} assumes that the core to star efficiency does not depend on the mass of the core or on the number of stellar objects formed.

The fraction of individual main-sequence stars formed with masses over $m_h \sim 8 M_\odot$ can be estimated as

$$F_{h,ms} \simeq \frac{R_{s,h} \mathcal{N}(m_{core} > R_{s,h} m_h / \epsilon)}{R_s \mathcal{N}(m_{core} > m_{bd} / \epsilon)}, \quad (17)$$

where $R_{s,h}$ is the mean number of high-mass stars ($m > m_h$) formed in high mass cores ($m_{core} > R_{s,h} m_h / \epsilon$). The values quoted in Table 2 correspond to $R_s \simeq 1.3$ and $R_{s,h} \simeq 2$. Note that eq.(17) assumes that the stellar system formed in a core does not disaggregate. Additionally, eq.(17) neglects the high-mass primary stars in systems with companions having masses below m_h . However, the error introduced is small because most high mass stars have a companion of similar mass (Maíz Apellániz 2008). Eq.(17) also neglects very low-mass primaries with brown dwarf companions ($m < m_{bd} \simeq 0.08 M_\odot$). Nonetheless, since the binary fraction of very low-mass stars is small ~ 0.2 (Reid et al. 2006; Burgasser et al. 2007), the vast majority of systems with $m > m_{bd}$ have main sequence primaries. Parravano et al. (2011) estimate that $F_{h,ms} \simeq (7 - 8) \times 10^{-3}$.

For seven values of the Hurst exponent H , Table 2 summarizes the average properties of the cores formed in sets of 20 simulations of fBm clouds with the same mass M_{cl} but a different setup of the random Fourier phases. For the parameter values used for the

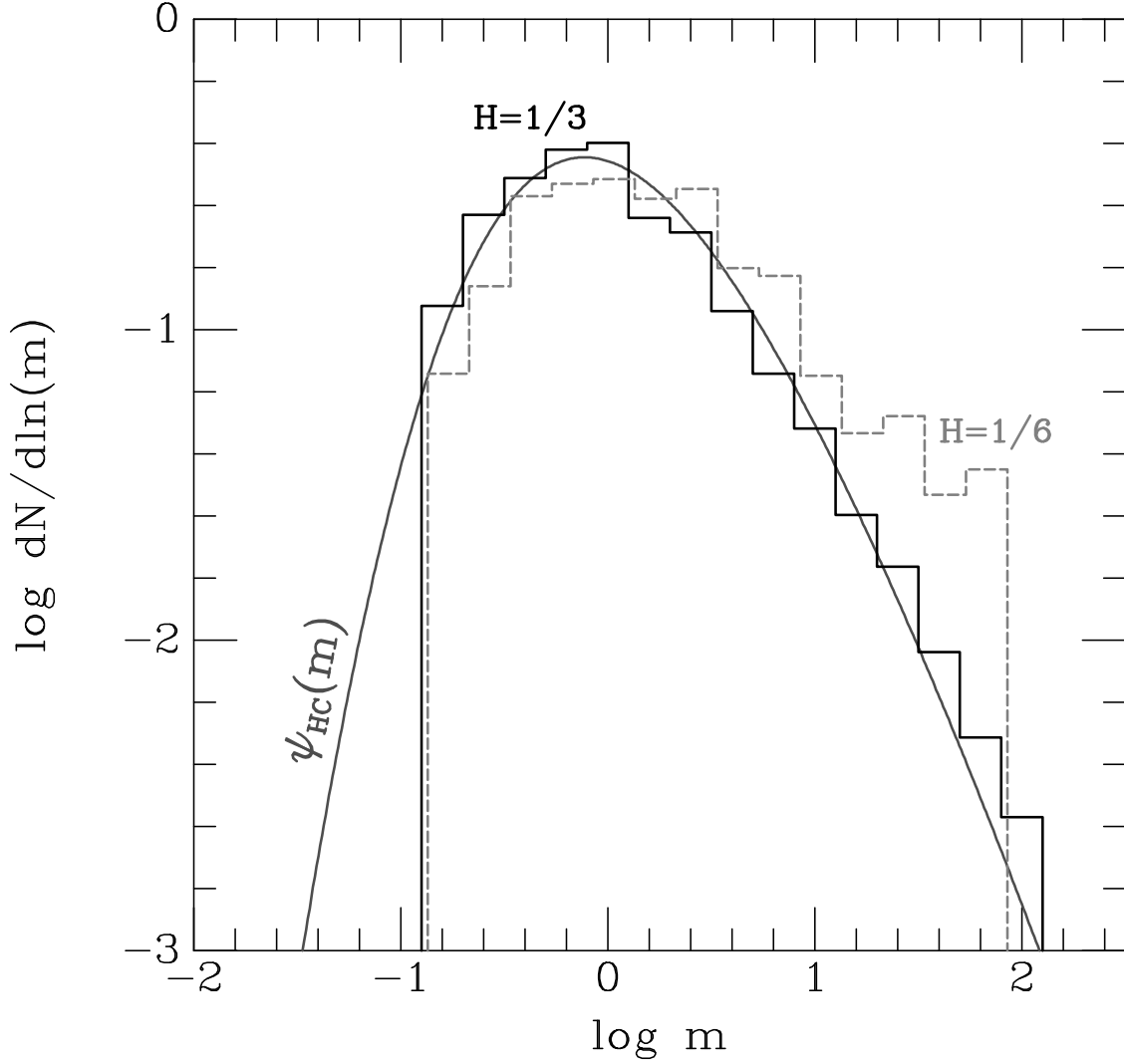


Fig. 4.— Mass distribution of the cores formed in a total of 20 different simulations of fBm clouds. The solid (dashed) line histogram corresponds to the mass function of fBm clouds with $H = 1/3$ ($H = 1/6$). The parameter values in all simulations are $N_{vox} = 2^8$, $m_{max} = 0.07 M_{\odot}$, $T = 10$ K and $\mu = 2.33$. The contrast factor α in each simulation is adjusted to produce a cloud with a mass of $860 M_{\odot}$ that corresponds to these parameter values (see third line in Table1). As in Fig. (2), the sharp rise at core mass of about $0.1 M_{\odot}$ is due to the adopted m_{max} value. The continuous curve shows $\psi_{HC}(m)$ for these parameter values.

TABLE 2
Average properties of the cores in fBm clouds

H	\mathcal{N}_{cores}^a	\bar{m}_{core}^b	$F_{m,c/g}^c$	$F_{h,ms}^d$
0	28 ± 6	16.28 ± 4.90	0.49 ± 0.06	0.13 ± 0.05
1/6	89 ± 25	5.07 ± 1.96	0.47 ± 0.06	0.022 ± 0.02
1/5	101 ± 29	4.47 ± 1.78	0.47 ± 0.07	0.017 ± 0.013
1/4	132 ± 38	3.43 ± 1.43	0.47 ± 0.06	0.009 ± 0.009
1/3	201 ± 57	2.42 ± 0.87	0.51 ± 0.06	0.005 ± 0.005
1/2	405 ± 110	1.31 ± 0.42	0.57 ± 0.06	0.0006 ± 0.0015
3/4	797 ± 177	0.76 ± 0.17	0.67 ± 0.05	0.0000 ± 0.0000

For each value of H , the values quoted correspond to the average over 20 simulations of fBm clouds with different random phase but identical parameter values $N_{vox} = 2^8$, $m_{max} = 0.07 M_\odot$, $T = 10K$, $\mu = 2.33$ and $\eta = 0.4$, that correspond to $L = 2.7$ pc, $M_{cl} = 860 M_\odot$, $\sigma_0 = 1.64$, as in the third case in Table 1. The errors indicate the standard deviation of the 20 values of each parameter for each value of H

^aNumber of cores per cloud.

^bAverage mass of cores in a cloud in solar masses.

^cFraction of the mass of the cloud that collapses in cores.

^dFraction of stars with masses over $8 M_\odot$ estimated with eq. (17).

simulations in Table 2, fBm clouds with $1/4 \lesssim H \lesssim 1/3$ produce an average core mass distribution that agrees both with the theoretical HC08 CMF and with the expected values of $\bar{m}_{core} \approx 3M_{\odot}$ and $F_{h,ms} \simeq (7 - 8) \times 10^{-3}$. Note also that as H increases the number of cores increases and their average mass decreases. Figure (5) shows the dependence of the relative variation of the number of cores $\Delta\mathcal{N}_{cores}/\mathcal{N}_{cores}$ as function of H , where $\Delta\mathcal{N}_{cores}$ is the standard deviation of \mathcal{N}_{cores} in the 20 simulations. Except for $H = 0$ the variations in the number of cores largely exceed the expected $\sqrt{\mathcal{N}}$ statistical variations. The analysis of the dependence of these variations on the considered physical processes and cloud structure is out of the scope of the present study. However, we notice here that for a fixed volume of simulation and a constant cloud mass the relative variation $\Delta N/N$ is about constant for fBm clouds with H values in the range considered in Fig. 5.

4.1. Spatial distribution of cores

The spatial distribution of the collapsing cores can be characterized by the surface density of companions (SDC) measured on a 2d projection of the positions of the cores by sampling all pair of cores over bins of separation ΔR . In order to compare with the SDC in young clusters (Simon 1997) we assume that half of the cores fragment to form two stars with 3D separations $\Delta R \leq l_{vox}$ following a probability distribution $p(R) \propto \Delta R^{-1/2}$. Figure (6) shows the surface density of companions for a single simulation of a fBm cloud with $H=1/3$ and the same parameter values used in Fig. (4) and the case $H=1/3$ in Table 2. The labeled power-laws in Fig. (6) are the SDCs reported by Simon (1997) for the Orion Trapezium star formation region and for the Ophiuchus star formation region. The SDC for this particular simulation is in between the observed SDC's for these two regions. The fall of the SDC at large radii is due to edge effects when ΔR is of the order of size L of the simulation. For other simulations with the same parameter values the SDCs are similar, but when the parameter H is increased the SDC curves shift upwards.

5. Conclusions

We have proposed a procedure to obtain the prestellar core mass distribution that results from the collapse of prestellar cores in clumps by assuming that the densest regions collapse first and form the smaller objects. At small scales, thermal support dominates and determines the mass distribution of cores at low masses, whereas at the largest scales turbulence dominates the support and determines the mass distribution at high masses. The numerical method proposed here make use of a small number of parameters, namely N_{vox}, T, μ, η , to-

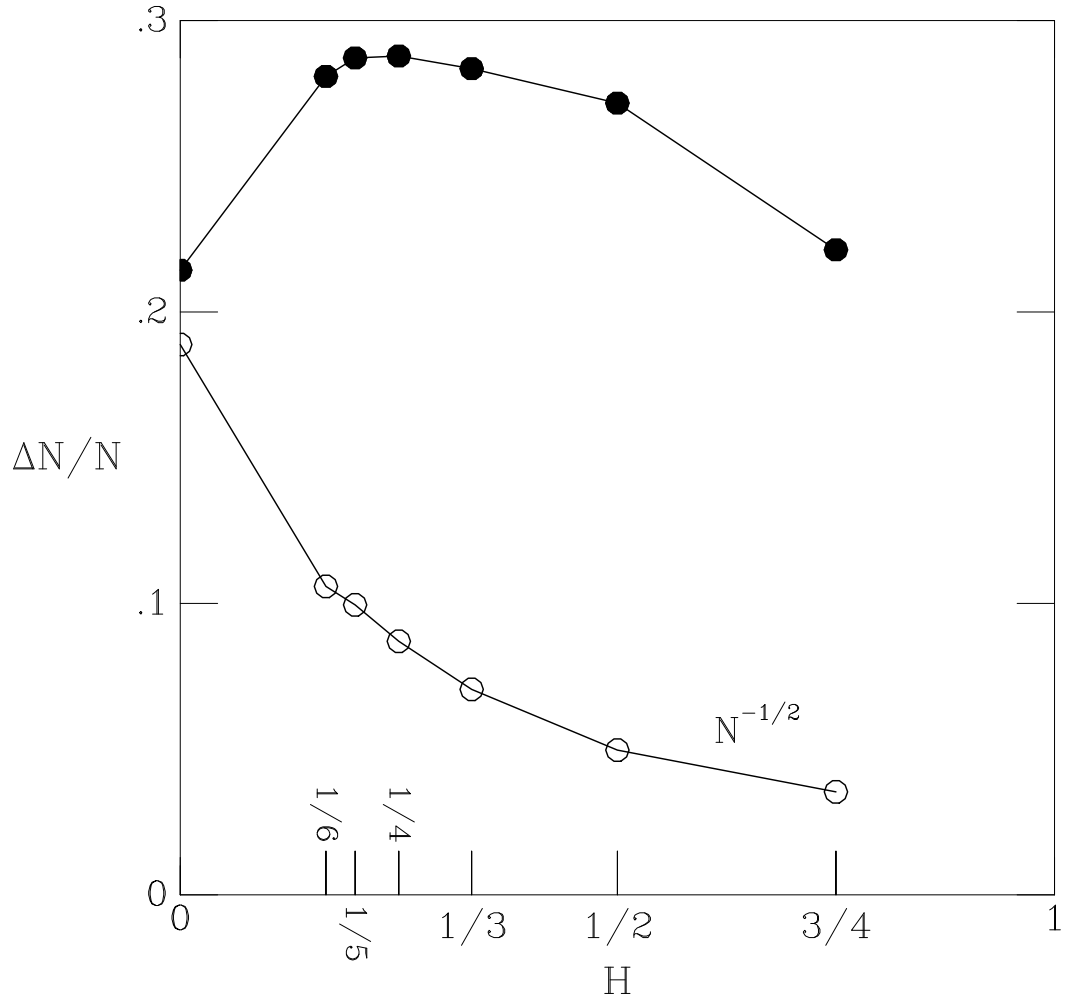


Fig. 5.— Relative variation of the number of cores ($\Delta\mathcal{N}_{cores}/\mathcal{N}_{cores}$) in 20 simulations as function of the Hurst parameter H . The open circles are the corresponding values $1/\sqrt{\mathcal{N}}$ expected if they were statistical variations of the number of cores.

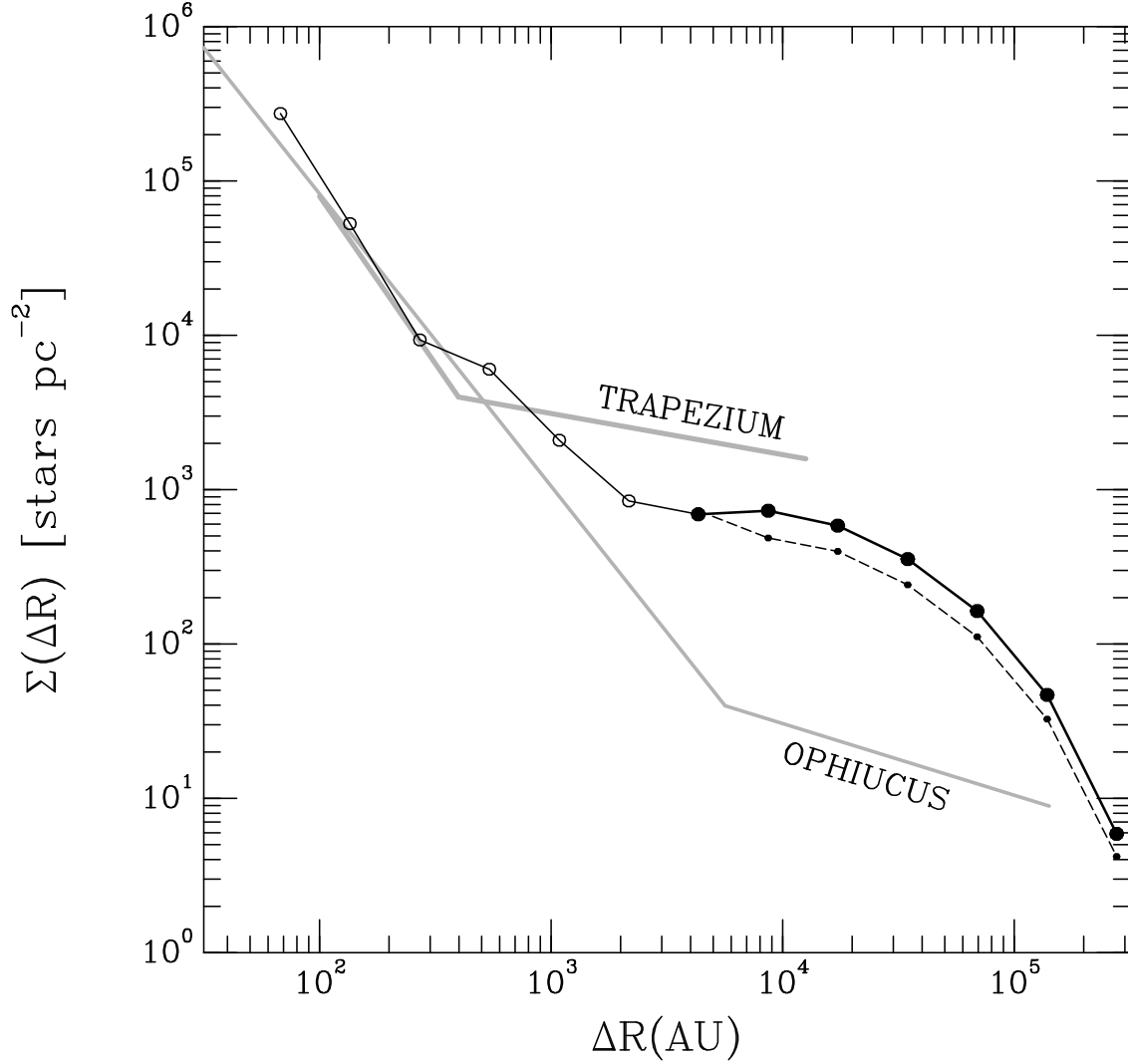


Fig. 6.— Surface density of companions $\Sigma(\Delta R)$ vs the separation in AU for a single simulation of fBm clouds with $H=1/3$. The small dots connected by dashed lines correspond to $\Sigma(\Delta R)$ for the cores. The large dots connected by solid lines correspond to the surface density of companions systems ($\Delta R > l_{vox}$) when half of the cores are assumed to fragment into two units. The open circles connected by light lines correspond to the surface density of companion stars assuming that the binary separation ΔR is less than l_{vox} with a probability distribution $p(R) \propto \Delta R^{-1/2}$. The two segment power-law gray lines represent the surface density of companions for the Orion Trapezium and Ophiuchus star formation regions (Simon 1997).

gether with the cloud properties (i.e. M_{cl} and H) and the assumptions that the mass in the densest voxel m_{max} is equal to the Jeans mass and that the cloud as a whole is marginally stable. When the proposed method is applied to a mass distribution whose density PDF is a log-normal at all smoothing scales R and its standard deviation $\sigma(R)$ is given by eq. (7), the average mass distribution agrees with the CMF predicted by the analytical theory of the IMF proposed by HC08. The HCS method can be seen as a numerical version of the HC08 theory, and there is univocal correspondence between the parameters in both models.

Both the Padoan-Nordlund IMF and the Hennebelle-Chabrier IMF apply to particular star-forming cloud conditions. In order to determine an average IMF that can be compared with observations of stars from different clouds, it is necessary to average their theoretical IMFs for a distribution of cloud temperatures, densities and Mach numbers. The core mass distribution from our method is even more dependent on cloud property since, as we have shown, the masses of the resulting cores also depend on the particular distribution of mass within the cloud. Large variations in the resulting core mass distribution are observed in fBm clouds with the same mass M_{cl} and Hurst exponent H , but a different setup of the random Fourier phases. As shown in Table 2 and Fig. (5), the number of cores in a set of 20 simulations display variations that largely exceed the expected \sqrt{N} statistical variations. Due to its simplicity the HCS method is computationally efficient at obtaining the mass and position of the cores that collapse in an arbitrary distribution of gas. Therefore the HCS method is well suited to analyzing the effects produced by changes in the physics over a large number of initial conditions.

We have applied the HCS method to lattices with a number of cells up to $2^{8 \times 3}$, which represent clumps of mass $\sim 10^3 M_{\odot}$ and size ~ 3 pc, but larger lattices can be processed. There is no restriction in the way the mass in the voxels is assigned, but we have focused on fBm clouds that have been used as analogs of real interstellar clouds. We confirm that fBm clouds with $H \simeq 1/3$, corresponding to $\gamma = 11/3$ (Elmegreen 2002), give better agreement with the theoretical CMF derived by Hennebelle and Chabrier and the observed IMF. We have also shown that the spatial distribution of the cores for fBm clouds with $H = 1/3$ has a surface density of companions that resembles that of young stellar clusters (Simon 1997). Since the HCS method provides the sequence and location of newly formed stars, the method can be easily modified to consider radiative feedback effects.

We wish to thank David Hollenbach and Christopher McKee for their valuable comments. AP was supported as guest researcher for part of this research by the IESA-CSIC. N.S. acknowledges financial support from the Ministerio de Economía y Competitividad of Spain through grant AYA2011-29754-C03-01, and EJA through grant AYA2010-17631.

REFERENCES

- Adams, F. C. & Fatuzzo, M., 1996, *ApJ*, 464, 256
- Alves, J., Lombardi, M. & Lada, C. J., 2007, *A&A*, 462, L17
- Bastian, N., Covey, K.R., Meyer, M.R., 2010, *ARA&A*, 48, 339
- Bate, M. R., 2009, *MNRAS*, 397, 232
- Bate, M. R., 2012, *MNRAS*, 419, 3115
- Bergin, E. A. & Tafalla, M., 2007, *ARA&A*, 45, 339
- Bertoldi, F. & McKee, C. F., 1992, *ApJ*, 395, 140
- Burgasser, A. J., Reid, I. N., Siegler, N., Close, L., Allen, P., Lowrance, P., & Gizis, J. 2007, *Protostars and Planets V*, 427
- Chabrier, G., & Hennebelle, P. 2010, *ApJ*, 725, L79
- Dib S., Piau L., Mohanty S., Braine J., 2011, *MNRAS*, 415, 3439
- Elmegreen, B. G. & Falgarone, E., 1996, *ApJ*, 471, 816
- Elmegreen, B. G. 1997, *ApJ*, 486, 944
- Elmegreen, B. G. 1999, *ApJ*, 515, 323
- Elmegreen, B. G. 2002, *ApJ*, 564, 773
- Elmegreen, B. G. & Scalo, J. 2004, *ARA&A*, 42, 211
- Elmegreen, B. G. 2010, *IAU Symposium*, 266, 3 (arXiv:0910.4638)
- Elmegreen, B. G. 2011, *Computational Star Formation*, 270, 407
- Falgarone, E., Puget, J.-L., & Perault, M. 1992, *A&A*, 257, 715
- Enoch, M. L., Evans, N. J., II, Sargent, A. I., et al., 2008, *ApJ*, 684, 1240
- Federrath, C., Klessen, R. S., Schmidt, W. 2009, *ApJ*, 692, 364
- Federrath, C., Roman-Duval, J., Klessen, R. S., Schmidt, W., Mac Low, M. M., 2010, *A&A*, 512, 81
- Girichidis, P., Federrath, C., Banerjee, R., & Klessen, R. S. 2011, *MNRAS*, 413, 2741

- Girichidis, P., Federrath, C., Banerjee, R., & Klessen, R. S. 2012a, MNRAS, 420, 613
- Girichidis, P., Federrath, C., Allison, R., Banerjee, R., & Klessen, R. S. 2012b, MNRAS, 420, 3264
- Gorti, U., & Hollenbach, D. J. 2002, ApJ, 573, 215
- Hennebelle, P., & Chabrier, G. 2008, ApJ, 684, 395
- Hennebelle, P., & Chabrier, G. 2009, ApJ, 702, 1428
- Hollenbach, D.J. & Tielens, A.G.G.M. 1999 Rev. Mod. Phys. 71, 173
- Inutsuka, S. 2001, ApJ, 559, L149
- Kainulainen, J., Beuther, H., Henning, T., Plume, R., 2009 A&A, 508, 35
- Kainulainen, J., Beuther, H., Banerjee, R., Federrath, C., Henning, T., 2011, A&A, 530, 64
- Kauffmann, J., Pillai, T., Shetty, R., Myers, P. C., Goodman, A. A., 2010, ApJ, 716, 433
- Kritsuk, A. G., Norman, M. L., Padoan, P., & Wagner, R. 2007, ApJ, 665, 416
- Kroupa, P. 2002, Science, 295, 82
- Krumholz, M. R., Klein, R. I., & McKee, C. F. 2007, ApJ, 656, 959
- Krumholz, M. R., Klein, R. I. & McKee, C. F. 2011 arXiv:1104.2038
- Lada, C. J. 2006, ApJ, 640, L63
- Larson, R.B. 1981, MNRAS, 194, 809
- Maíz Apellániz, J. 2008, ApJ, 677, 1278
- Matzner, C. D. & McKee, C. F. 2000, ApJ, 545, 364
- McKee, C. F., & Ostriker, E. C. 2007, ARA&A, 45, 565
- McKee, C. F., & Tan, J. C. 2003, ApJ, 585, 850
- Michel, M., Kirk, H. & Myers, P. C., 2011, ApJ, 735, 51
- Miville-Deschenes, M. A., Levrier, F. & Falgarone, E. ApJ, 593, 831
- Motte, F., Andre, P., & Neri, R. 1998, A&A, 336, 150

- Myers, P. C., & Fuller, G. A., 1992, *ApJ*, 396, 631
- Nordlund, Å. K., & Padoan, P. 1999, in *Interstellar Turbulence*, ed. J. Franco & Carramiñna (Cambridge: Cambridge Univ. Press), 218
- Ostriker, E. C., Stone, J. M., & Gammie, C. F. 2001, *ApJ*, 546, 980
- Padoan, P., Nordlund, Å. & Jones, B. J. T. 1997, *MNRAS*, 288, 145
- Padoan, P. & Nordlund, Å. 2002, *ApJ*, 576, 870
- Padoan, P., & Nordlund, Å. 2004, *ApJ*, 617, 559
- Padoan, P., Nordlund, Å., Kritsuk, A. G., Norman, M. L., & Li, P. S. 2007, *ApJ*, 661, 972
- Parravano, A., McKee, C. F., & Hollenbach, D. J. 2011, *ApJ*, 726, 27
- Passot, T., & Vázquez-Semadeni, E., 1998, *Phys. Rev. E*, 58, 4501
- Press, W. H., & Schechter, P. 1974, *ApJ*, 187, 425
- Price, D. J., & Bate, M. R., 2009, *MNRAS*, 398, 33
- Reid, I. N., Lewitus, E., Allen, P. R., Cruz, K. L., & Burgasser, A. J. 2006, *AJ*, 132, 891
- Salpeter, E., 1955, *ApJ*, 121, 161
- Sánchez, N. & Parravano, A. 1999, *ApJ*, 510, 795
- Sánchez, N., Alfaro, E. J., Pérez, E., 2005, *ApJ*, 625, 849
- Sánchez, N., Alfaro, E. J., Pérez, E., 2006, *ApJ*, 641, 347
- Sánchez, N., Alfaro, E. J., Elias, F., Delgado, A. J. & Cabrera-Cano, J., 2007a, *ApJ*, 667, 213
- Sánchez, N., Alfaro, Pérez, E., 2007b, *ApJ*, 656, 222
- Sánchez, N., Añez, Ne., Alfaro, E. J. & Odekon, M. C. 2010, *ApJ*, 720, 541
- Shadmehri, M., & Elmegreen B. G. 2011, *MNRAS*, 410, 788
- Scalo, J. M. 1998, in *The Stellar Initial Mass Function*, Proceedings of the 38th Herstmonceux Conference, ed. G. Gilmore & D. Howell. ASP Conference Series, Vol. 142, 1998, p.201
- Schmidt, W., Federrath, C., Hupp, M., Kern, S., Niemeyer, J. C., 2009, *A&A*, 494, 127

- Schmidt, W., Kern, S. A. W., Federrath, C., Klessen, R. S., 2010, *A&A*, 516, 25
- Simon, M., 1997, *ApJ*, 482, L84
- Stutzki, J., Bensch, F., Heithausen, A., Ossenkopf, V., Zielinsky, M., 1998, *A&A*, 336, 697
- Testi, L. & Sargent, A. I. 1998, *ApJ*, 508, L91
- Vázquez-Semadeni, E., 1994, *ApJ*, 423, 681